Traffic 2006; **7:** 1333–1351
Blackwell Munksgaard

doi: 10.1111/j.1600-0854.2006.00476.x

Antagonistic Forces Generated by Cytoplasmic Dynein and Myosin-II during Growth Cone Turning and Axonal Retraction

Kenneth A. Myers[1], Irina Tint[1,2], C. Vidya Nadar[1], Yan He[1], Mark M. Black[2,3] and Peter W. Baas[1,3,*]

[1]Department of Neurobiology and Anatomy, Drexel University College of Medicine, Philadelphia, PA 19129, USA
[2]Department of Anatomy and Cell Biology, Temple University School of Medicine, Philadelphia, PA 19140, USA
[3]These senior authors contributed equally to this study
**Corresponding author: Peter W. Baas, pbaas@drexelmed.edu*

Cytoplasmic dynein transports short microtubules down the axon in part by pushing against the actin cytoskeleton. Recent studies have suggested that comparable dynein-driven forces may impinge upon the longer microtubules within the axon. Here, we examined a potential role for these forces on axonal retraction and growth cone turning in neurons partially depleted of dynein heavy chain (DHC) by small interfering RNA. While DHC-depleted axons grew at normal rates, they retracted far more robustly in response to donors of nitric oxide than control axons, and their growth cones failed to efficiently turn in response to substrate borders. Live cell imaging of dynamic microtubule tips showed that microtubules in DHC-depleted growth cones were largely confined to the central zone, with very few extending into filopodia. Even under conditions of suppressed microtubule dynamics, DHC depletion impaired the capacity of microtubules to advance into the peripheral zone of the growth cone, indicating a direct role for dynein-driven forces on the distribution of the microtubules. These effects were all reversed by inhibition of myosin-II forces, which are known to underlie the retrograde flow of actin in the growth cone and the contractility of the cortical actin during axonal retraction. Our results are consistent with a model whereby dynein-driven forces enable microtubules to overcome myosin-II-driven forces, both in the axonal shaft and within the growth cone. These dynein-driven forces oppose the tendency of the axon to retract and permit microtubules to advance into the peripheral zone of the growth cone so that they can invade filopodia.

Key words: actin, axon, cytoplasmic dynein, EB3, growth cone, microtubule, myosin-II, neuron

Received 17 February 2006, revised and accepted for publication 19 July 2006, published on-line 15 August 2006

Microtubules form a continuous array within the axon, extending from the cell body along the axonal shaft and into the growth cone. Within the array, individual microtubules assume a variety of lengths, from a few microns to over a hundred microns (1–3). Recent studies have established that only the shortest microtubules within the array undergo rapid concerted transport (4). The longer microtubules are essentially immobile (5,6). The transport of the short microtubules is intermittent, rapid and bidirectional. We have reported that cytoplasmic dynein is an important motor for transporting these short microtubules (6,7) and that it does so by pushing against either longer microtubules or actin filaments (8). It seems improbable that motor proteins would be selective for short microtubules; hence, we have speculated that cytoplasmic dynein generates forces against microtubules of all lengths but only transports the short microtubules (9). The dynein-driven forces on long microtubules may be important for their alignment and interaction with the same substrates against which the shorter microtubules are transported, namely other microtubules and the actin cytoskeleton.

Interactions between microtubules and actin filaments are important for a number of different aspects of axonal development. For example, axonal retraction is known to result from contraction of the cortical actin (10,11), which is offset by compression-bearing microtubules within the axonal shaft (12). Within the growth cone, long microtubules originating in the central zone (or within the axonal shaft) extend into the peripheral zone by assembling along the straight bundles of actin filaments within filopodia [for review, see reference (13)]. Entry of microtubules into filopodia is necessary for the growth cone to navigate properly in response to environmental cues (13–19). Over the years, a variety of non-motor proteins have been suggested to regulate the interactions between microtubules and actin filaments in the axon and growth cone [for review, see reference (20)]. For example, molecules such as MAP2c form static cross-links between the two filament systems (21), and regulatory molecules such as small G-proteins influence the assembly of both filaments [for review, see reference (22)]. By contrast, little attention has focused on how forces generated by molecular motors might integrate the two filament systems.

We previously reported that acute disruption of dynactin causes poorly adhered axons to retract but not if myosin-II is also inhibited (23). We interpreted these findings as

reflecting an antagonistic relationship between the forces generated by cytoplasmic dynein and myosin-II. However, since these studies were performed, it has become known that dynactin interacts with a variety of other motor and non-motor proteins in addition to cytoplasmic dynein (24,25). Hence, it is unclear whether these results of dynactin disruption can be attributed to dynein-driven forces, as we speculated at the time. In this study, we have further pursued the issue of axonal retraction using small interfering RNA (siRNA) to deplete dynein heavy chain (DHC). In addition, we sought to determine whether a similar antagonism between cytoplasmic dynein and myosin-II might regulate microtubule advance into peripheral regions of the growth cone and promote their entry into filopodia, both of which are necessary for proper growth cone turning in response to substrate cues.

Results

We previously reported that siRNA effectively depletes DHC from cultured rat sympathetic neurons (6,7). The siRNA is introduced at the time of plating, and the levels of protein gradually drop over a period of a few days thereafter. By day 2, the levels of DHC are diminished by over 70%, while at days 3–4, the levels are diminished by 80–90%. Interestingly, there is no noticeable change in the rates of axonal growth as the DHC is depleted, although this is hard to assess past the second day because of the length and complexity of the axonal arbors. Also, the general morphology of the axons is similar to controls. These results were somewhat surprising given that cytoplasmic dynein is a multifunctional motor with roles in a variety of processes such as organelle transport, distribution of Golgi elements, neurofilament transport and microtubule transport (26). More recently, we found that axonal growth rates are stunted if the neurons are depleted of DHC for 3–4 days and then replated to allow them to grow axons anew (6). Under these conditions, the axons were not only significantly shorter but also displayed abnormal microtubule organization, particularly in their most distal regions. Specifically, the microtubules were not aligned paraxially, but rather displayed a criss-crossed quilt-like pattern, and virtually never extended into filopodia. This result suggested to us that forces generated by cytoplasmic dynein may be important for aligning microtubules with one another and for their invasion into the actin-rich peripheral zone of the growth cone. However, given that the axons were stunted in their growth, it was unclear whether the defects in microtubule organization were secondary to the inhibition of growth.

One way to avoid this complication is to study the neurons at a point during dynein depletion at which they grow axons at relatively normal rates. This would allow us to evaluate whether a reduction in dynein levels can have subtle effects on aspects of axonal development such as retraction and growth cone turning that are not secondary to a slowing of axonal growth. We found that when neurons were replated after only 2 days of dynein depletion, axons grew anew at rates indistinguishable from neurons treated similarly with control siRNA, at least over the subsequent $\approx$15 h. Specifically, at 15 h after replating, the axons of control and dynein-depleted neurons were 492 ± 222 μm and 484 ± 147 μm in length, respectively (mean $\pm$ SD, $n = 17$ for both groups), which corresponds to average axonal growth rates of 33 and 32 μm/h, respectively. Neurons treated in this fashion were used for all of the studies presented here, together with control neurons treated identically but with control siRNA. As described below, the dynein deficiency produced with this approach, while not altering axonal growth rate, markedly enhanced axonal retraction, suppressed growth cone turning and suppressed microtubule invasion into filopodia.

Dynein depletion increases the degree of axonal retraction induced by nitric oxide

To ascertain whether there are effects of dynein depletion on the tendency of axons to retract, we treated cultures with the nitric oxide donor, NOC-7, after the axons had exceeded 100 μm in length. In previous studies, we reported that axons retracted as a result of application of NOC-7 and that such retraction involved the retreat of microtubules rather than their depolymerization (27). The morphologies of neurons immediately before and 30 min after exposure to nitric oxide were recorded by phase-contrast microscopy. By 30 min after nitric oxide treatment, the percentages of axons that had retracted $\geq$5 μm were 45% and 83% for the control and DHC-depleted neurons, respectively (Figure 1G). Dynein-depleted axons retracted 37 μm on average, significantly more than did the control axons, which retracted 17 μm on average (Figure 1H). In time-lapse, phase-contrast images, control axons exhibited typical retraction morphologies, characterized by a retraction bulb, a thin, distal trailing remnant and sinusoidal bends along the axonal shaft (Figure 1A,B), similar to what we observed previously (27). Retracting dynein-depleted axons showed similar morphological features during retraction (Figure 1D,E). Microtubule staining showed the abundant presence of microtubules in all retracted axons (Figure 1C,F). As in our previous studies (23,27), microtubules showed no depolymerization but instead were reconfigured into coiled and bended arrays (Figure 1F, inset).

In our previous study, showing that acute disruption of dynactin results in axonal retraction, we found that prior inhibition of myosin-II prevented the retraction from occurring (23). In that study, we microinjected n-ethylmaleimide-modified myosin heads to inhibit myosin-II function. Since then, a far simpler method for inhibiting myosin-II has emerged, namely application of a membrane-permeable drug called blebbistatin (10,28). Here, we treated the neurons for 30 min with 50 μM blebbistatin prior to adding the NOC-7. No retraction was observed either in the control or in the dynein-depleted axons, consistent with previous studies, indicating that axonal retraction requires myosin-II-based contractility of the cortical actin (10,11). Taken

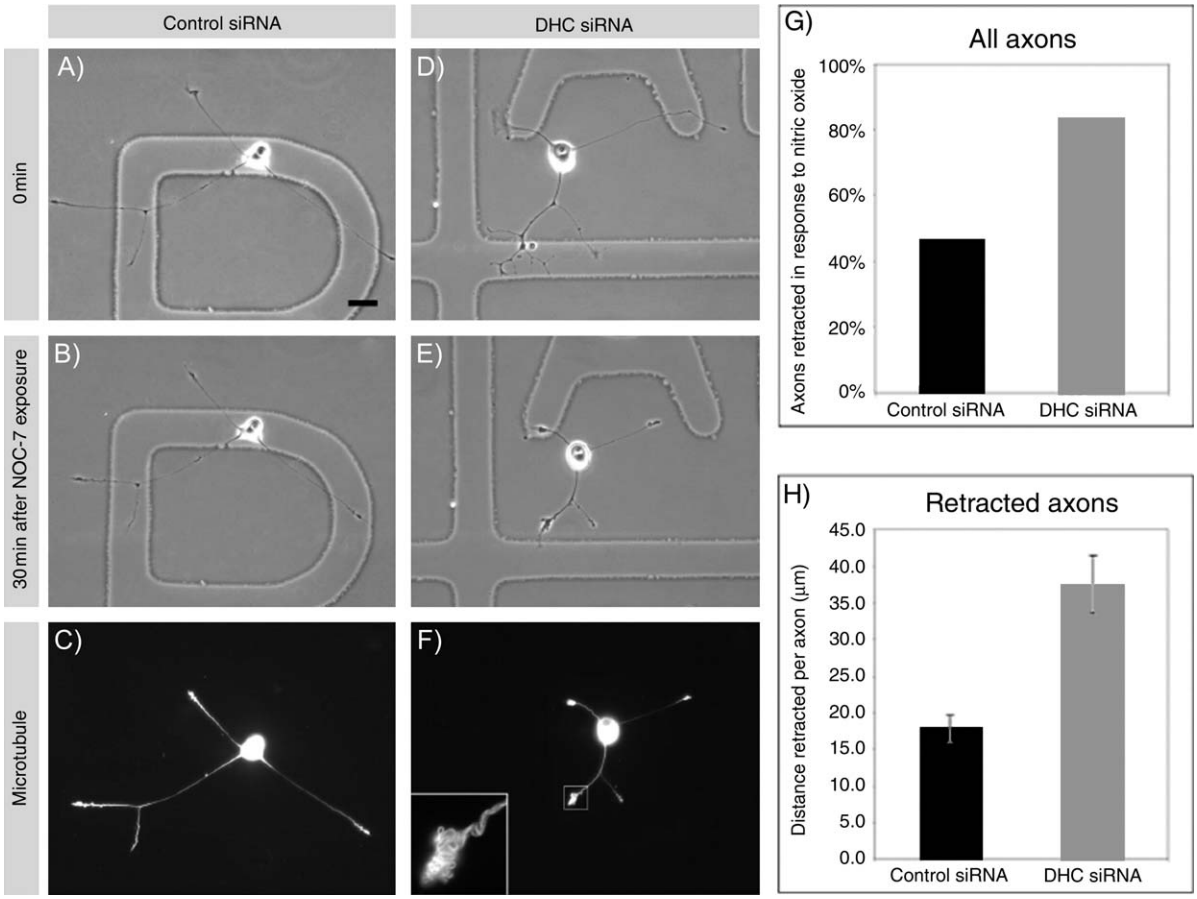

Figure 1: Dynein depletion enhances nitric oxide-induced axonal retraction. Phase-contrast images show neuronal morphologies immediately before (A and D) and 30 min after (B and E) exposure to a nitric oxide donor. A control-siRNA-treated neuron (A and B) retracted its axons over significant distances in response to nitric oxide, showing typical 'retraction bulbs' at axon tips (described in *Results*). However, a DHC-depleted neuron (D and E) retracted its axons over much greater distances than the control neuron and showed more dramatic retraction bulbs at axon tips. Panels (C) and (F) are the microtubule staining of the control neuron and the DHC-depleted neuron, respectively. In both cases, microtubules are abundant in retracted axons and appear as coiled arrays with no apparent depolymerization during the retraction (see inset in F). G) Quantification of the percentage of axons retracted in response to nitric oxide among control and DHC-depleted neurons. H) The average distance (in microns) retracted per axon is quantified and compared among different groups of neurons. Distances retracted by DHC-depleted axons are approximately two times greater than those in control neurons (*$p < 0.05$, two-tailed *t*-test). Bar, 10 μm.

together, these results on axonal retraction are consistent with our previous interpretation, namely that forces generated by cytoplasmic dynein offset or antagonize forces generated by myosin-II to prevent axonal retraction (12,23)].

Growth cones display defects in turning after dynein depletion

To determine whether the growth cones of dynein-depleted axons display deficits in their ability to turn, we used a patterned substrate consisting of alternating stripes of laminin-containing and laminin-free zones (28,29). Because the laminin-free zones provide a poor substrate for growth, when growth cones of elongating axons reach borders between laminin-containing and laminin-free zones, typically they change their direction of growth to remain on laminin. For quantitative analyses, cultures were fixed and stained to reveal the laminin stripes, microtubules and actin filaments. Figure 2 shows examples of growth cones of control-siRNA-treated neurons at borders between laminin-containing and laminin-free zones. Figure 2 A–D shows examples of growth cones that underwent turning at the border, while Figure 2E–H shows examples of growth cones that failed to turn. In many situations, turning was complete at the time of fixation and appeared as a relatively abrupt change in axonal orientation at or near the border (Figure 2A,B). In other situations, growth cones were situated at borders without a clear change in axonal orientation, and in these cases, the appearance of the microtubule array was used to evaluate whether growth cones were turning (Figure 2C,D) or not turning (Figure 2 E–H) (see *Materials and Methods*). When assayed in this manner, dynein depletion significantly retarded growth cone turning (Figure 2I, Table 1 panel A). Roughly 60% of control growth cones turned at borders, whereas only

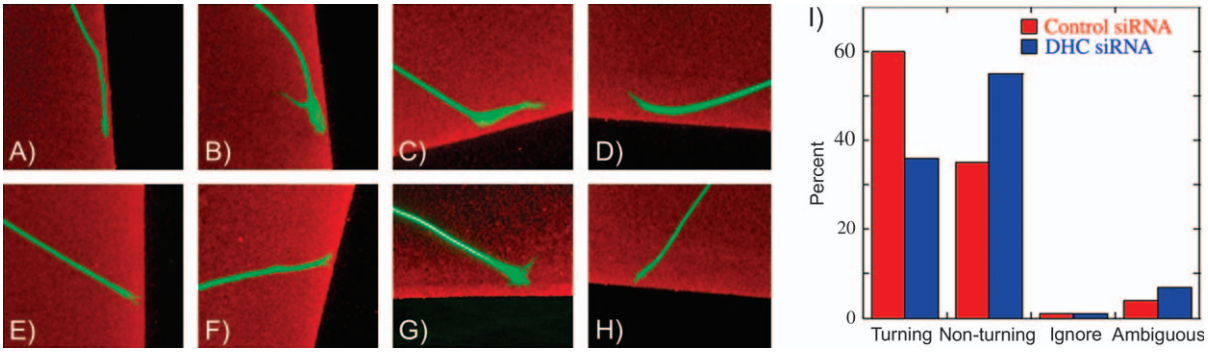

Figure 2: Growth cone turning is diminished in dynein-depleted growth cones. Growth cone behaviors of control neurons (A–H). Neurons cultured after transfection with control or DHC siRNA for 2 days were replated onto patterned laminin substrates and allowed to extend axons for ≈15 h. The cultures were then fixed and stained for laminin (red) and microtubules (green), and growth cones at borders between laminin-containing and laminin-free zones were imaged and then scored for turning as described in the text. The figure shows examples of control growth cones scored as turning (A–D) or not turning (E–H). Categorization and quantification of growth cone turning revealed a 58% reduction in the frequency of turning in DHC-depleted growth cones compared to control-siRNA-treated growth cones (I). Bar, 8.3 μm.

Table 1: Dynein depletion reduces the frequency of growth cone turning and alters the configuration of growth cone microtubules

A. Growth cone turning behavior

	Growth cone behavior				
	Turning (%)	Non-turning (%)	Ignore (%)	Unclear (%)	p
All growth cones (*n*)					
DHC siRNA (363)	35	55	2	7	<0.0001
Control siRNA (328)	60	35	1	4	
Spread growth cones					
DHC siRNA (222)	43	48	1	8	<0.0001
Control siRNA (288)	61	34	1	4	
Blunt growth cones (*n*)					
DHC siRNA (141)	26	67	2	5	<0.002
Control siRNA (40)	58	40	0	2	

B. Growth cone microtubule configuration parameters

	Proportion of growth cones having filopodia with microtubules, % (*n*)	Microtubule area/growth cone area mean ± SD (*n*)
Control siRNA	50 (105)	0.229 ± 0.071 (34)
DHC siRNA	26 (49)	0.176 ± 0.074 (40)
p	<0.001	0.0027

A) Growth cone turning behavior. Growth cones at borders between laminin-containing and laminin-free zones were scored as turning or non-turning; growth cones that elongated onto the laminin-free zones are indicated as ignore, and growth cones that could not be clearly categorized as turning, non-turning or ignore are indicated as unclear. These designations were made for the total population of growth cones analysed and also for those growth cones categorized as spread or blunt as described in the text, and the resulting data were evaluated statistically with the chi-square test. B) Growth cone microtubule configuration parameters. We determined the proportion of control and dynein-depleted growth cones that had one or more filopodia with microtubules. Approximately one half of the images available for these analyses were examined and, to avoid bias, the images were selected from the image list prior to viewing, and all growth cones in each image were evaluated (we scored 210 control growth cones and 186 dynein-depleted growth cones). See Materials and Methods for further detail.

35% of growth cones of dynein-depleted neurons turned ($p < 0.0001$, chi-square test). The fact that growth cone turning was not completely eliminated may suggest that dynein is not absolutely necessary for turning. Alternatively, it may be that dynein is absolutely required for growth cone turning but that the levels of dynein remaining with our siRNA regimen are sufficient to allow for some amount of turning.

It is our hypothesis (see below) that growth cones use dynein-driven forces to overcome forces generated by myosin-II and that this antagonistic force relationship

underlies growth cone turning. However, it is also possible that turning might be stunted in DHC-depleted cones due to other abnormalities such as an accumulation of vesicles and neurofilaments that can also occur as a result of dynein depletion (6,7). Growth cones that are particularly rich in vesicles and/or neurofilaments are generally more blunt in appearance (6). In dynein-depleted cultures, some growth cones were spread, while others showed the more blunt morphology. Spread and blunt growth cones also appeared in control cultures, but the spread morphologies predominated more so in controls than in dynein-depleted cultures. In the experiment shown in Table 1 panel A, 12% of the growth cones in the control-siRNA-treated cultures had the blunt appearance, whereas 39% had this appearance in the dynein-depleted cultures. Both spread and blunt growth cones showed filopodia and lamellipodia as seen by phalloidin staining (Figure 3). The microtubules in the blunt cones formed a dense tangle in the central region of the growth cone (Figure 3A,C) rather than the splayed configuration typical of spread growth cones (Figure 3B,D). Control growth cones with a spread or blunt appearance exhibit similar turning behavior in our assay (Table 1 panel A) and are statistically indistinguishable from each other ($p > 0.1$, chi-square test). In dynein-depleted cultures, both spread and blunt growth cones were significantly impaired at turning (Table 1 panel A). Blunt growth cones in dynein-depleted cultures turned less frequently than spread growth cones ($p < 0.0001$, chi-square test), suggesting that the effects of dynein depletion that lead to the blunt morphology of growth cones also impact their ability to turn. However, the fact that spread growth cones in dynein-depleted cultures also turn poorly indicates that the turning deficit is not simply a manifestation of the factors that transform a growth cone from a spread to a blunt morphology.

Microtubule distribution is abnormal in dynein-depleted growth cones

We next examined the distribution of microtubules relative to actin filaments in control and dynein-depleted growth cones of neurons grown on the stripe preparation. In both control and dynein-depleted growth cones (Figure 3), microtubules extend from the axon into the central region of the cone. In control growth cones, the microtubules typically splay as they enter the cone and one or more commonly extend from the central domain of the cone into the peripheral domain and align with actin bundles of filopodia. In dynein-depleted growth cones, microtubules appear much less splayed within the central domain and examples of microtubules that extend into the peripheral domain and align with actin bundles of filopodia are much less common than in controls. These visual impressions were confirmed quantitatively (Figure 4, Table 1 panel B). Dynein depletion reduced

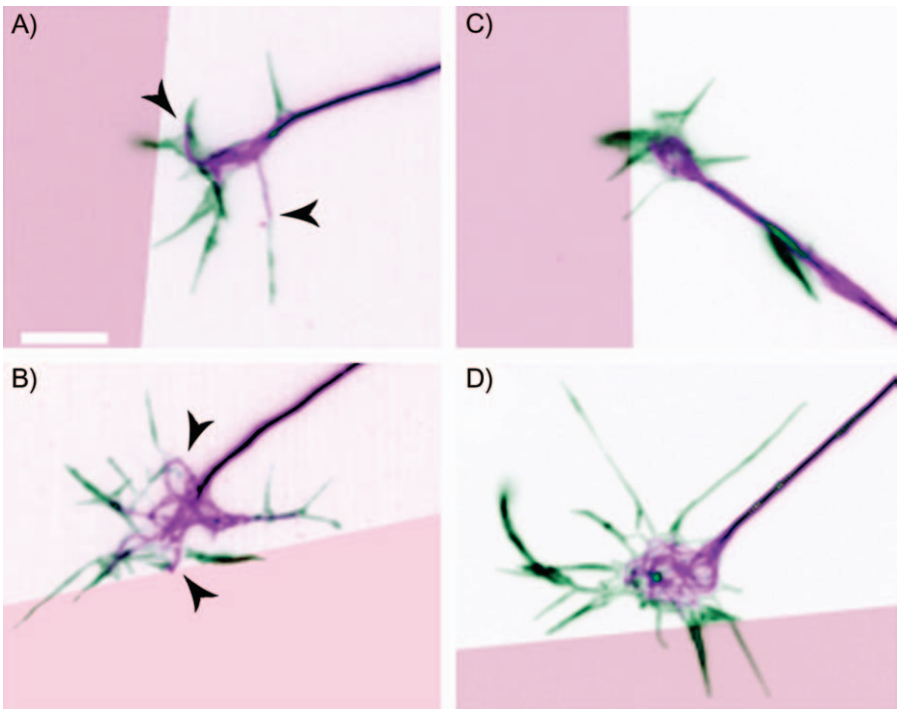

Figure 3: Representative growth cones at borders of laminin-containing and laminin-free zones stained to reveal microtubules (purple), actin filaments (green), and laminin (laminin-free zones are dark pink). In control growth cones (A and B), microtubules extend from the central domain of the growth cone into the peripheral domain and align with actin bundles of filopodia (arrowheads in A and B). In contrast, in dynein-depleted growth cones (C and D), microtubules are confined to the central domain, and examples of microtubules extending into the peripheral domain and aligning with actin bundles of filopodia are much less common than in controls. A) and C) are examples of non-spread growth cones, whereas (B) and (D) are examples of spread growth cones. Bar, 8.3 μm.

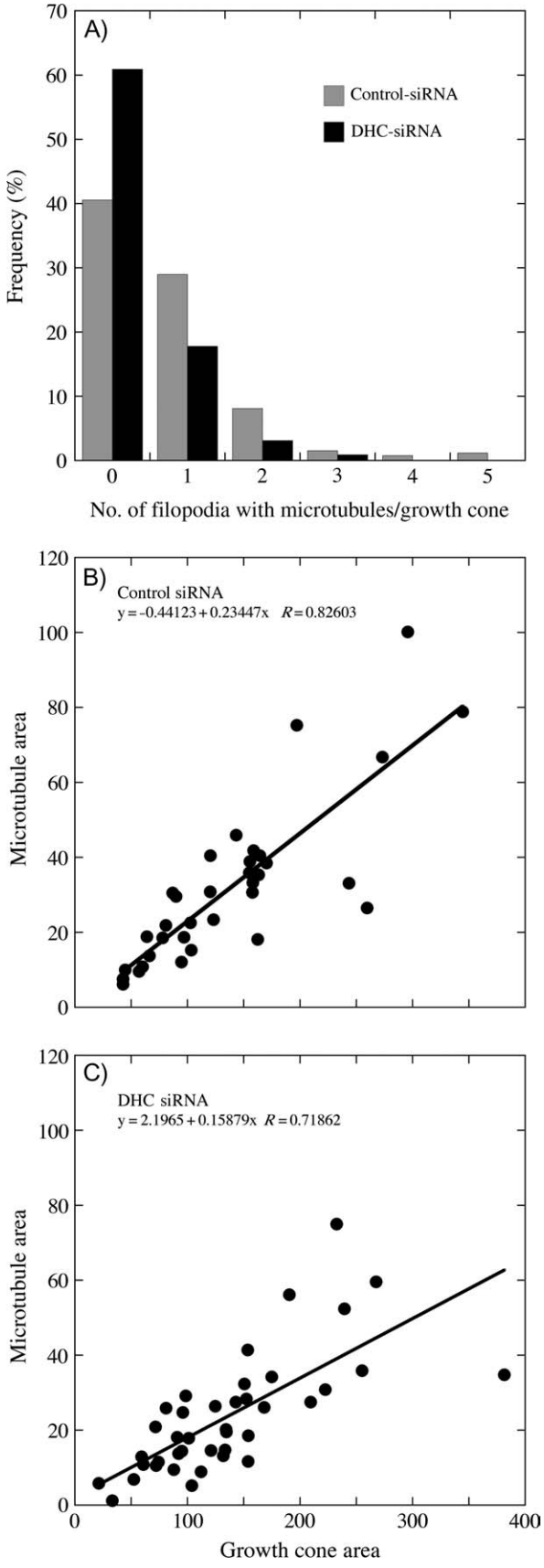

Figure 4: Quantitative analyses on effects of dynein depletion on growth cone microtubules. A) Frequency histogram of the number of filopodia with microtubules per growth cone for control and dynein-deficient neurons. The data were obtained as described in the Table 1 panel B. The number of filopodia/growth cone that contained microtubules ranged from zero to five in the samples examined (210 control growth cones and 186 dynein-depleted neurons), and over this entire range, growth cones of dynein-depleted neurons had significantly fewer filopodia with microtubules compared to those of control-siRNA treated neurons ($p < 0.001$). B) and C) Linear regression analyses relating the area occupied by microtubules in the growth cone to total growth cone area in control (B) and dynein-depleted (C) neurons. These area measurements were calculated as described in the *Materials and Methods*. Note that the area occupied by the microtubule array increased linearly with growth cone area, and this was true for both control and dynein-depleted growth cones. However, the slope of the line for control growth cones is ≈1.5 times greater than that for dynein-depleted growth cones, indicating that microtubules occupy a greater proportion of growth cone area in control neurons compared to dynein-depleted neurons.

the proportion of total growth cone area occupied by microtubules by ≈25% ($p < 0.003$, Student's *t*-test), and counts of the number of growth cones in which microtubules were present in one or more filopodia revealed ∼50% reduction in dynein-depleted growth cones compared with controls.

EGFP-EB3 reveals defects in microtubule behavior in dynein-depleted growth cones

On the basis of these results, it is possible that microtubules enter filopodia as frequently in dynein-depleted and control growth cones, but in the absence of dynein, they reside in filopodia for much shorter times. The other possibility is that microtubules simply do not enter the filopodia as effectively in the absence of dynein. To distinguish between these possibilities, we examined the behavior of EB3 'comets' generated by expression of EGFP-EB3 in these neurons (8,30). EB3 is one member of a category of proteins called +TIPs that associate with microtubule plus ends during assembly [for discussion, see references (30,31)]. The excursion of the EGFP-EB3 at the plus end of the microtubule appears as a moving comet because of the gradual dissociation of EB3 molecules from the microtubule as it continues to add more subunits (thus producing a comet-shaped burst of fluorescence with its tail toward the minus end of the microtubule).

In control neurons, EB3 comets emanated in all directions from the central zone of the growth cone and invaded virtually all the filopodia down their entire lengths (Figure 5A and Movie S1). By contrast, in dynein-depleted growth cones, EB3 comets were almost never observed beyond the central zone of the cone, and very few were ever observed within filopodia (Figure 5B, Movie S2). Mean EB3 comet numbers per filopodium were 4.22 in controls and 0.48 in dynein-depleted growth cones, with 75% of the dynein-depleted filopodia having zero EB3 comets

(Figure 5C). These results, showing a major deficiency in the capacity of microtubules to enter filopodia of dynein-depleted growth cones, appear to be even more dramatic than those observed on the fixed neurons, possibly because EB3 only reveals a sub-fraction of the total microtubule population or possibly because of the different manner by which the data were collected for each study.

The few comets that did enter the filopodia of dynein-depleted growth cones displayed shorter excursion distances compared to the comets within the filopodia of control growth cones, and these differences were statistically significant ($p < 0.05$, two-tailed Student's *t*-test; Figure 5D). EB3 comet velocities in both control and dynein-depleted growth cones were slower than previously reported comet velocities recorded within the axon (6,8,30). Even so, EB3 excursion velocities within dynein-depleted growth cones were reduced by 32% compared to EB3 excursion velocities measured in control growth cones (Figure 5E). EB3 velocities were 0.095 μm/seconds in controls and 0.065 μm/seconds in dynein-depleted growth cones, a difference that was statistically significant ($p < 0.00001$, two-tailed Student's *t*-test).

Inhibition of myosin-II permits microtubules to invade filopodia of dynein-depleted growth cones

One explanation for the results described above is that an opposing force resists the entry of microtubules into filopodia and that this force is too strong for the microtubules to overcome in the absence of dynein. As noted previously, it is our hypothesis that this opposing force is driven by myosin-II. In this regard, the actin filaments within filopodia tend to move backward, especially when the growth cone is not moving (32), and this retrograde flow of actin can direct microtubules away from filopodia (for discussion, see reference (13)). The retrograde flow, which is partially attenuated when filopodia make attachments to the substrate and when the growth cone advances (33,34), is driven by myosin-II (35). In addition, myosin-II generates traction forces during growth cone advance (34,36,37).

Before studying the effects of myosin-II inhibition on microtubule behaviors in DHC-depleted growth cones, we first wished to verify that the dynein depletion itself was not affecting rates of retrograde actin flow. For this, we observed retrograde flow using polystyrene beads essentially as previously described (35). Under this experimental regimen, the rates of the bead movements were found to be nearly identical in both control siRNA and DHC siRNA growth cones. The retrograde flow velocity for control neurons was 0.063 ± 0.002 μm/min [mean ± standard error of the mean (SEM), $n = 47$], while the retrograde flow velocity for DHC-depleted neurons was 0.059 ± 0.006 μm/min (mean ± SEM, $n = 51$), values that did not represent a statistically significant difference ($p = 0.53$, two-tailed Student's *t*-test) (Figure 6).

To investigate a potential role for myosin-II in suppressing microtubule invasion into filopodia of dynein-depleted growth cones, we treated neurons with 50 μM blebbistatin. Initially, we double stained the cultures for actin and microtubules, as described previously. With vehicle alone, dynein-depleted growth cones displayed actin that was normally distributed and microtubules that were generally twisted and confined to the central zone of the cone (Figure 7A). After 30 min of blebbistatin treatment, the actin was also normally distributed, but now the microtubules were no longer twisted, and they extended forward into the peripheral zone to invade virtually every actin-rich extension or filopodium (Figure 7B/b,C/c). These results are consistent with the hypothesis that myosin-II provides the opposing force that prevents microtubules from effectively entering the peripheral zone and filopodia when dynein is depleted.

We next performed live cell imaging of the behaviors of the microtubules. For these experiments, we used a monomeric Red Fluorescent Protein (mRFP) labeled EB3 because blebbistatin cannot be used in conjunction with EGFP due to the fact that the excitation wavelength causes photodamage in the presence of the drug (38). We found that while the mRFP-EB3 comets were not as sharp in the images and bleached faster, their behavior was essentially identical to that of the EGFP-EB3 comets in terms of velocity and distribution. Figure 8A and Movie S3 show a dynein-depleted growth cone expressing mRFP-EB3; as with the EGFP-EB3, it is clear that the comets are confined to the central zone. Figure 8B and Movie S4 show a similar dynein-depleted growth cone but treated with blebbistatin. Under these conditions, the EB3 comets invade the filopodia and move at rapid rates that exceed those recorded in neurons treated with control siRNA alone. Quantification of EB3 comet invasion revealed that the frequency of invasion into blebbistatin-treated, dynein-depleted filopodia was 4.50 events/filopodium compared to 0.48 for neurons depleted of dynein alone and 2.58 for blebbistatin-treated control neurons (Figure 8C, Table 2).

Similar findings were obtained during evaluation of comet excursion depths, where again, either dynein depletion by itself or blebbistatin treatment alone reduced the depths of comet excursions; yet, the blebbistatin/dynein depletion combination produced a rescue of EB3 excursion depths, in this instance to levels even greater than those recorded in control growth cones. The mean comet excursion depth for blebbistatin-treated, dynein-depleted filopodia was 5.44 μm compared to 3.71 μm in blebbistatin-treated controls, while in neurons depleted of dynein alone, the mean excursion depth was 1.93 μm (Figures 8D and 5D, Table 2). Measurements of EB3 comet velocities revealed increased velocities in blebbistatin-treated, dynein-depleted growth cones compared to neurons depleted of dynein alone, but no significant difference was observed between control or dynein-depleted neurons when also treated with blebbistatin [mean ± SEM = 0.201 ± 0.013 μm/seconds

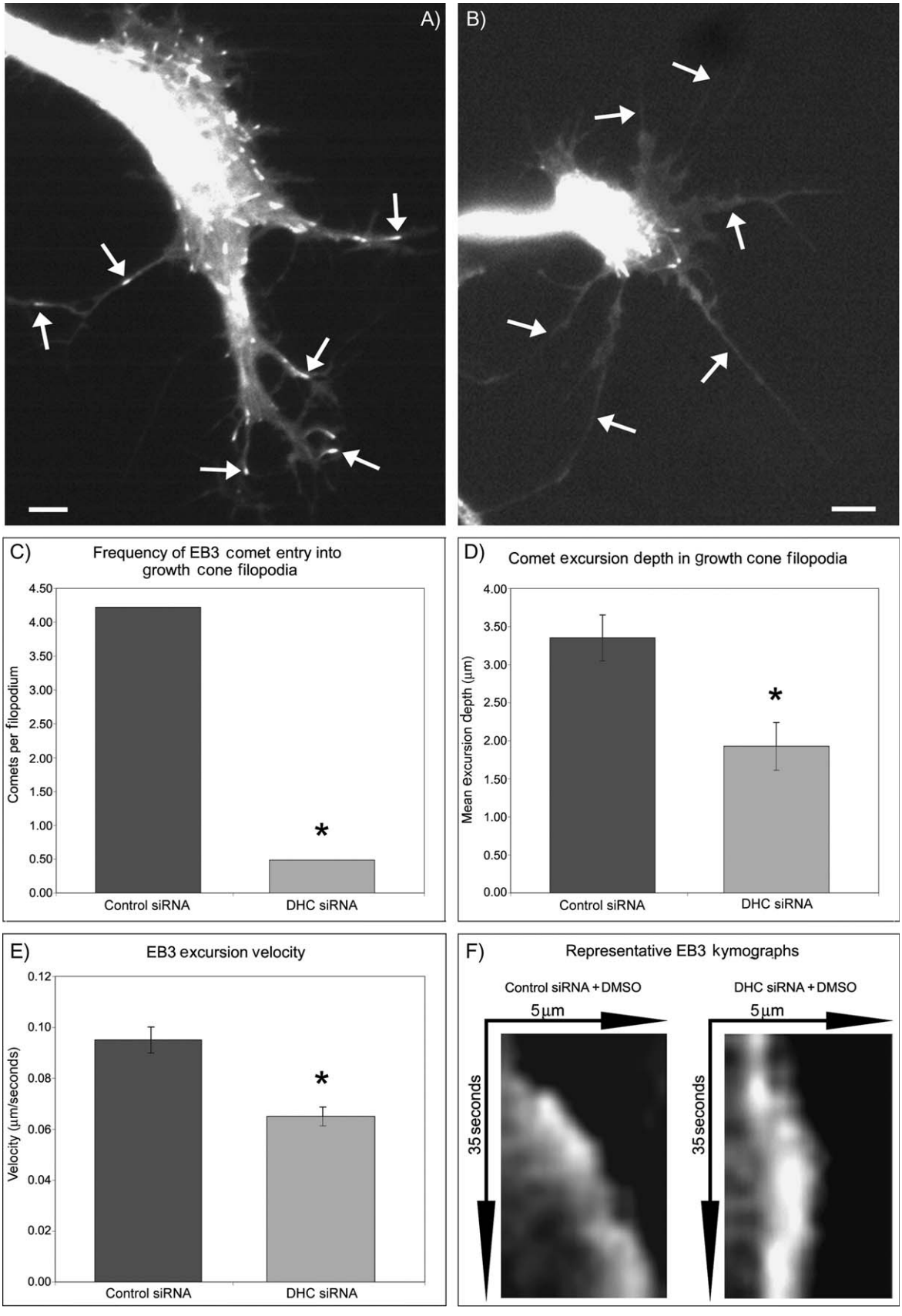
A)
B)
C)
Frequency of EB3 comet entry into growth cone filopodia
Comets per filopodium
4.50
4.00
3.50
3.00
2.50
2.00
1.50
1.00
0.50
0.00
*
Control siRNA
DHC siRNA
D)
Comet excursion depth in growth cone filopodia
Mean excursion depth (μm)
4.00
3.50
3.00
2.50
2.00
1.50
1.00
0.50
0.00
*
Control siRNA
DHC siRNA
E)
EB3 excursion velocity
Velocity (μm/seconds)
0.12
0.10
0.08
0.06
0.04
0.02
0.00
*
Control siRNA
DHC siRNA
F)
Representative EB3 kymographs
Control siRNA + DMSO
DHC siRNA + DMSO
5 μm
5 μm
35 seconds
35 seconds

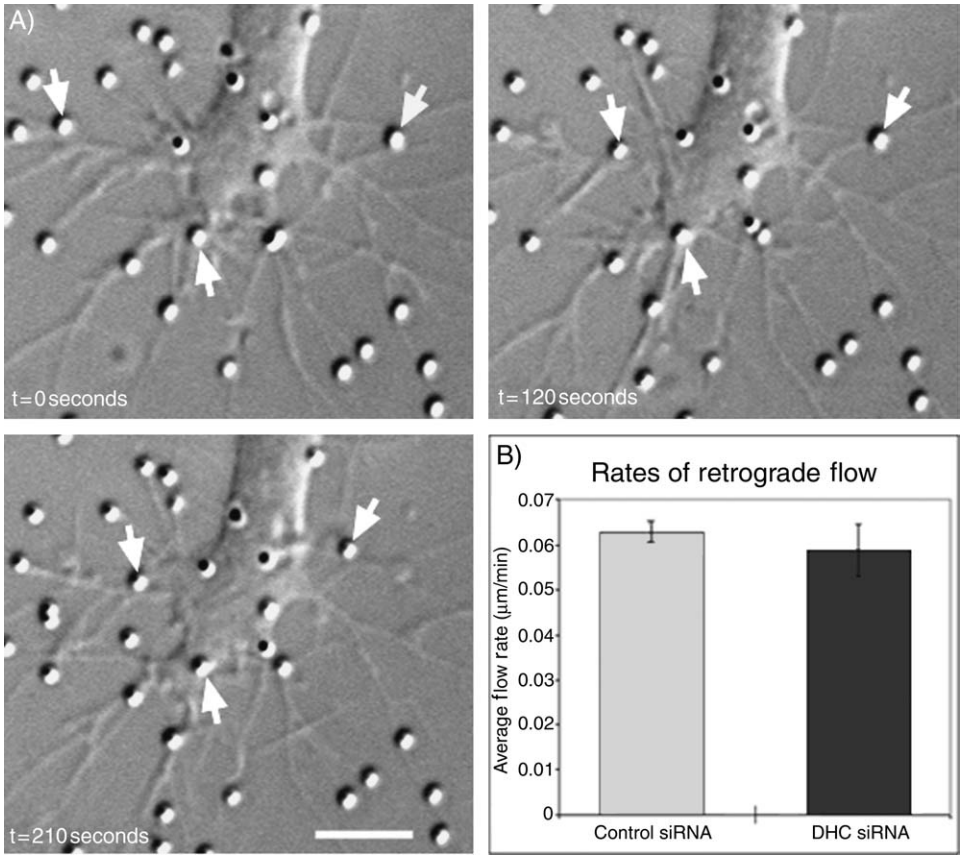

Figure 6: Depletion of DHC does not affect the rates of retrograde actin flow. A) Still-frame images extracted from live cell movies of a control-siRNA-treated growth cone. The three time-points depicted show the progressive movement of polyethylenamine-coated beads undergoing retrograde transport from the distal growth cone toward the central region of the growth cone. Arrows demarcate three beads that underwent substantial movement during the observed time period. B) Quantification of retrograde flow data revealed that there is no statistically significant variation in the velocities of retrograde movement in neurons treated with control or DHC siRNA ($p > 0.1$, two-tailed *t*-test; $n = 47$ control, $n = 51$ DHC). Arrows demarcating actin rich filopodia in the top panels were transcribed onto tubulin immunostaining images (bottom panels) to indicate microtubule/actin colocalization. Bar, 5 μm.

(control + blebbistatin) and 0.150 ± 0.008 μm/seconds (dynein depletion + blebbistatin)] (Figures 8E and 5E, Table 2). Interestingly, while the blebbistatin/control combination resulted in comet velocities that exceeded those of the blebbistatin/dynein depletion combination, under both of these experimental conditions, EB3 velocity measurements were similar to those recorded within elongating axons of uninhibited control axons (8,30).

We were initially surprised that blebbistatin treatment, within itself, had slightly deleterious effects on comet invasion into filopodia. However, this might relate to the fact that myosin-II contributes to the integrity of the actin bundles along which the microtubules invade (19). Even so, the fact that blebbistatin treatment entirely reverses the deleterious effects of dynein depletion provides strong support for the conclusion that myosin-II-driven forces

Figure 5: Microtubule advance and invasion of growth cone filopodia are markedly reduced in dynein-depleted growth cones. A) and B) Still-frame images extracted from live cell movies of a control siRNA (A) and DHC siRNA growth cone (B). In control growth cones, EGFP-EB3 comets frequently enter filopodia and commonly extend toward filopodia tips, while in dynein-depleted growth cones, EGFP-EB3 comets fail to enter filopodia (arrows in A and B). C) Quantification of filopodial invasion by EGFP-EB3 comets reveals a significant decrease in the frequency of microtubule entry into dynein-depleted growth cones over a 5-min imaging period (*, $p < 0.001$, chi-square analysis). D) Measurements of EB3 excursion depth reveal that, on the average, comet excursions proceed significantly farther toward the distal tip of growth cone filopodia in control-siRNA-treated neurons than do comet excursion in dynein-depleted neurons [*, $p < 0.05$, two-tailed Student's *t*-test; mean distance ± SEM = 2.500 ± 0.313 μm (control), and 1.433 ± 0.303 μm (DHC)]. E) Analysis of excursion velocities show that EB3 comets move significantly slower in dynein-depleted growth cones compared to control-siRNA-treated growth cones [*, $p < 0.00001$, two-tailed Student's *t*-test; mean velocity ± SEM = 0.095 ± 0.005 μm (control); 0.065 ± 0.004 μm (DHC)]. F) Kymographs of EGFP-EB3 excursion in neurons treated with control siRNA and DHC siRNA. In control growth cones, EB3 comets display progressive and consistent forward movements, while in dynein-depleted growth cones, EB3 comets remain near their starting positions, displaying bouts of assembly that are unable to advance the position of the polymerizing microtubule. Bar, 5 μm.

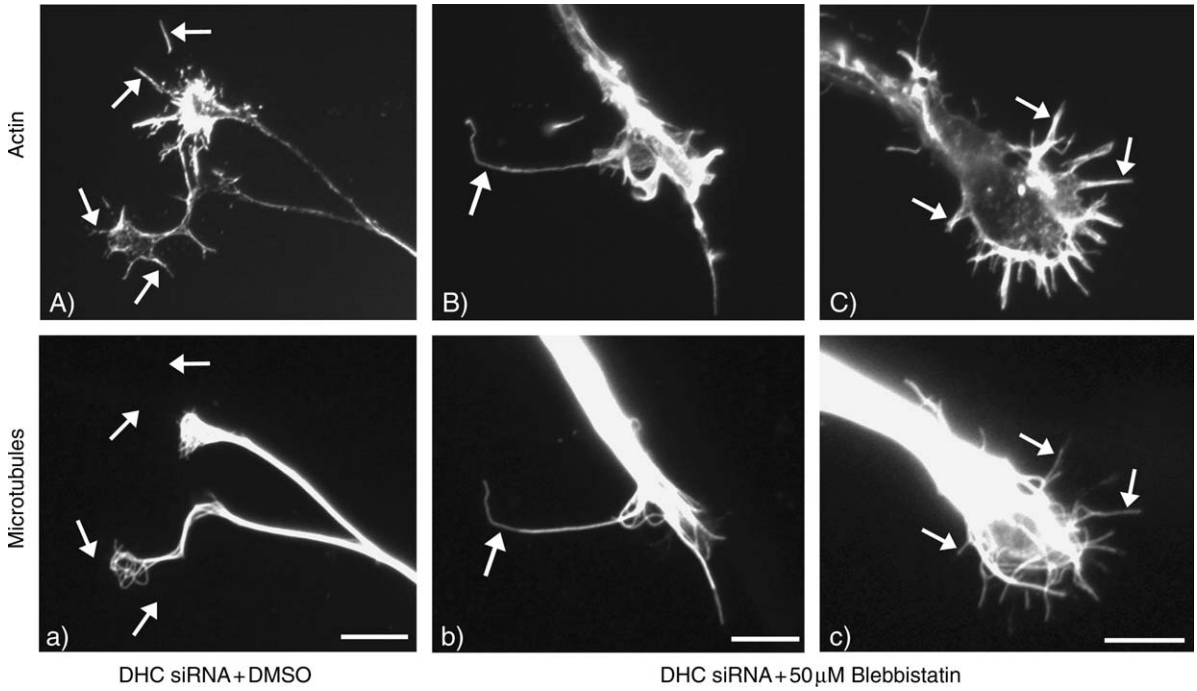

Figure 7: Inhibition of myosin-II results in alterations in microtubule organization in dynein-depleted growth cones. Neurons were depleted of DHC using siRNA and then treated with 50 μM blebbistatin for 30 min. Cultures were then double stained to reveal actin filaments (top panels) and microtubules (bottom panels). With vehicle (DMSO) alone, dynein-depleted growth cones displayed actin that was normally distributed (A) and microtubules that were generally twisted and confined to the central zone of the cone (a). After blebbistatin treatment, the microtubules were no longer twisted but extended forward into peripheral zone to invade virtually every actin-rich extension or filopodium (B/b/C/c). Arrows demarcating actin rich filopodia in the top panels were transcribed onto tubulin immunostaining images (bottom panels) to indicate microtubule/actin colocalization. Bars, 10 μm.

oppose the entry of microtubules into filopodia and that dynein-driven forces are normally used for the microtubules to overcome these myosin-II-driven forces.

Microtubule distribution in growth cones is also influenced by cytoplasmic dynein and myosin-II when microtubule dynamics are suppressed

Previous studies have shown that the entry of microtubules into filopodia is dependent upon the dynamic properties of the microtubules (33,39,40). If microtubule assembly is pharmacologically inhibited, the microtubules fail to enter the filopodia and the growth cone fails to turn. In light of these previous findings, the question arises as to how cytoplasmic dynein contributes to microtubule invasion of filopodia. One possibility is that the forces generated by the molecular motors are mainly important for the overall advance of the microtubule mass from the central zone into the peripheral zone (so that individual microtubules can then polymerize into filopodia). To gain more insight into this matter, we studied microtubule distribution

Figure 8: Inhibition of myosin-II relieves inhibition of microtubule advance into dynein-depleted growth cones and promotes microtubule invasion into filopodia. A) and B) Still-frame images extracted from live cell movies of a dynein-depleted (A) and dynein-depleted, blebbistatin-treated growth cone (B). In neurons depleted of dynein alone, mRFP-EB3 comets appear disoriented and fail to enter growth cone filopodia, while in dynein-depleted growth cones treated with blebbistatin, mRFP-EB3 comets regain the ability to enter growth cone filopodia (arrows in A and B). C) Analysis of mRFP-EB3 comet entry into filopodia revealed that the frequency of filopodial invasion in blebbistatin-treated, dynein-depleted growth cones is enhanced compared to growth cones treated with blebbistatin and control siRNA [frequency = 4.50 events/filopodium (DHC siRNA + blebbistatin), frequency = 2.58 events/filopodium (control siRNA + blebbistatin)]. These invasion frequencies are similar to those measured in neurons treated with control siRNA alone. D) The combination of dynein depletion and blebbistatin treatment resulted in excursion depths statistically similar to blebbistatin-treated control neurons [$p > 0.3$; 5.44 μm (DHC siRNA + blebbistatin); 3.71 μm (control siRNA + blebbistatin)]. E) mRFP-EB3 velocity analysis show that myosin-II inhibition increases comet velocities in both control and dynein-depleted growth cones when compared to siRNA treatment alone, while no significant difference is observed between controls and dynein-depleted growth cones that have been treated with blebbistatin [$p > 0.05$; mean ± SEM = 0.201 ± 0.013 μm (control + blebbistatin), and 0.150 ± 0.008 μm (DHC + blebbistatin)]. F) Kymographs of mRFP-EB3 comets reveal that blebbistatin treatment relieves the inhibition of microtubule advance observed when DHC is depleted; note that the kymograph of a comet after DHC depletion and blebbistatin treatment is similar to the kymographs after treatment with control siRNA alone (Figure 5F). Bar, 5 μm.

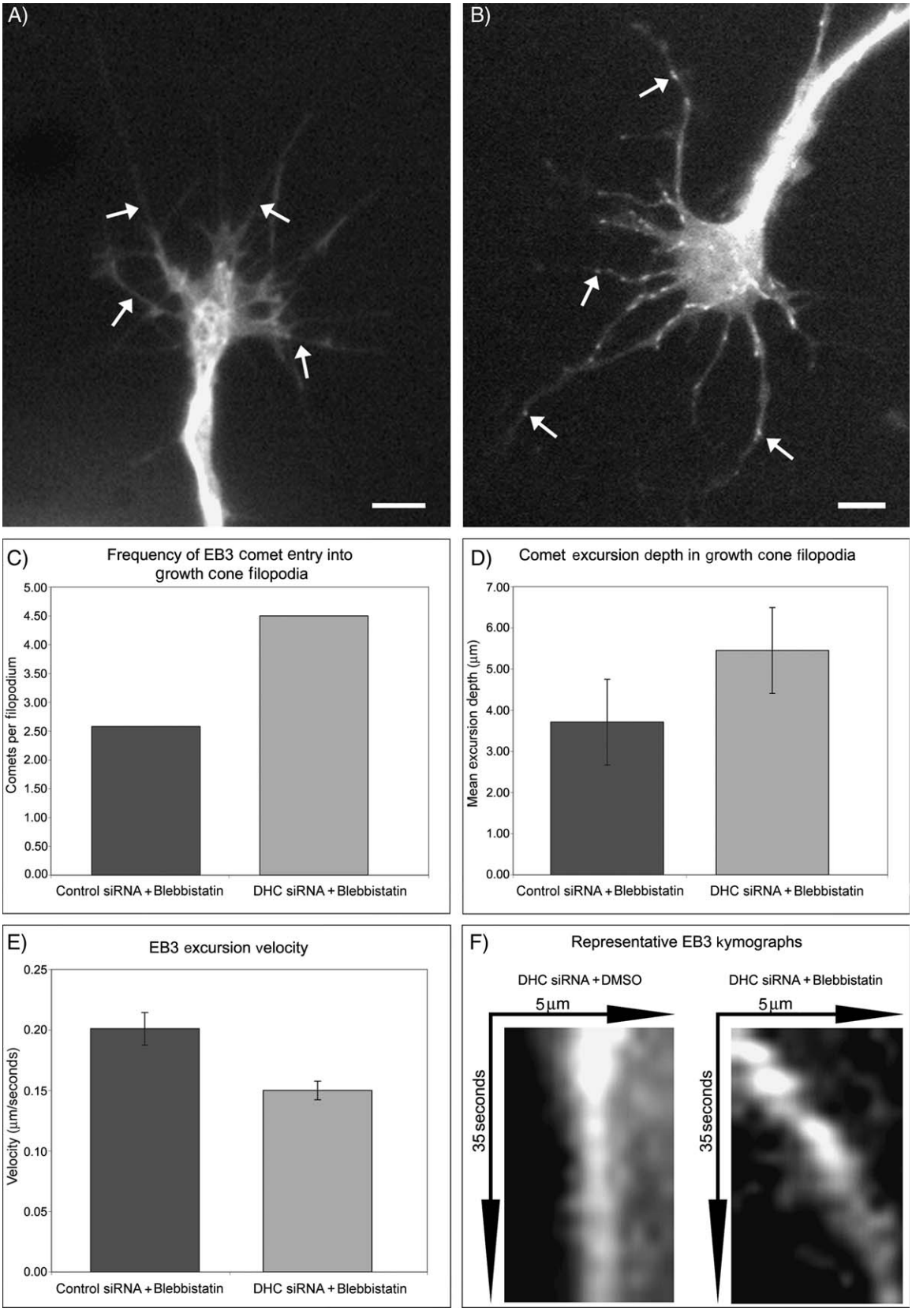
A)
B)
C)
Frequency of EB3 comet entry into growth cone filopodia
Comets per filopodium
5.00
4.50
4.00
3.50
3.00
2.50
2.00
1.50
1.00
0.50
0.00
Control siRNA + Blebbistatin
DHC siRNA + Blebbistatin
D)
Comet excursion depth in growth cone filopodia
Mean excursion depth (μm)
7.00
6.00
5.00
4.00
3.00
2.00
1.00
0.00
Control siRNA + Blebbistatin
DHC siRNA + Blebbistatin
E)
EB3 excursion velocity
Velocity (μm/seconds)
0.25
0.20
0.15
0.10
0.05
0.00
Control siRNA + Blebbistatin
DHC siRNA + Blebbistatin
F)
Representative EB3 kymographs
DHC siRNA + DMSO
DHC siRNA + Blebbistatin
5 μm
5 μm
35 seconds
35 seconds

Table 2: Effects of dynein depletion on microtubule invasion of filopodia and EB3 comet velocities within the growth cone. A) Data quantification showing the number of filopodia and the number of EB3 comets analysed for excursion depth. All filopodia that were 5 μm or greater in length were considered for the study. The mean excursion depth was calculated as the maximum distance that the comets traversed into the filopodia from the line of origin, which was drawn at the base of individual filopodia. B) EB3 comet distributions were analysed based on the number of comets that entered individual filopodia, and data were categorized into three groups consisting of filopodia with zero comets, filopodia with one to five comets and filopodia with more than five comets during the time of imaging. The same growth cones in (A) were used for quantitative analysis of EB3 comet velocities depicted in (C)

	Control siRNA, EGFP-EB3	DHC siRNA, EGFP-EB3	Control siRNA, mRFP-EB3 (Blebbistatin)	DHC siRNA, mRFP-EB3 (Blebbistatin)
A. EB3 comet number per filopodium and the mean EB3 excursion depth				
No. of filopodia	27	28	12	18
No. of comets	228	27	62	162
Comets per filopodia	4.22	0.48	2.58	4.50
Mean excursion depth (μm)	3.350	1.925	3.710	5.445
B. Filopodial comet distribution				
0, *n* (%)	3 (11)	21 (75)	0 (0)	0 (0)
1–5, *n* (%)	13 (48)	6 (21)	4 (67)	3 (17)
More than 5, *n* (%)	11 (41)	1 (4)	8 (33)	15 (83)
C. Mean EB3 comet velocities				
No. of comets	35	31	10	17
Mean velocity (μm/seconds)	0.095	0.065	0.201	0.150

in control and DHC-depleted growth cones treated with vinblastine to inhibit microtubule dynamics. Initially, we scored the frequency of EB3 comet appearances in growth cones in the presence of various concentrations of vinblastine and found that the concentrations as low as 0.05 nM resulted in a significant reduction (Figure 9E). Even so, we chose to use 50 nM vinblastine for our studies on dynein-depleted neurons because this higher concentration even further reduced comet frequency, and because we showed in previous studies that 50 nM vinblastine actually causes some depolymerization of microtubules, thus ensuring confidence that any redistribution of microtubules in the presence of the drug cannot be attributed to microtubule assembly (6,8,39).

As with the experiments presented previously, neurons were transfected with either control or DHC siRNA, allowed to grow axons for 2 days, and where then replated onto dishes coated with poly-D-lysine. The following morning, the cells had developed very short (<50 μm) axons, at which point they were exposed to vinblastine. After 30 min, laminin was then added to facilitate axonal growth. After 2 h, the neurons were fixed and stained for microtubules and actin, total growth cone area was calculated, and microtubule mass [arbitrary fluorescence units (AFU)] was determined for the distal 25% of each growth cone. We chose to define the distal region of the cone in this fashion because, under some of our experimental conditions, the demarcation between the central and the peripheral zones becomes somewhat ambiguous. As in the previous studies, we observed virtually no microtubules within filopodia. In neurons treated with control siRNA and vinblastine, microtubule mass was recorded at 43.0 ± 3.12 AFU (mean ± SEM, $n = 17$) in the distal region of the growth cone (Figure 9). In the case of neurons depleted of DHC, microtubule mass within the distal region of the growth cone was reduced to 18.8 ± 3.62 AFU (mean ± SEM, $n = 16$; $p < 0.00001$) for a statistically significant reduction of 43.7%. On this basis, we conclude that the forces generated by cytoplasmic dynein play a critical role in facilitating microtubule entry into the peripheral zone of the growth cone.

We next included myosin-II inhibition in the experimental regimen. These experiments were performed as described above, except that 30 min prior to fixation, cultures were treated with 50 μM blebbistatin. Data from these experiments revealed that, in neurons treated with control siRNA, vinblastine and blebbistatin, microtubule levels in the distal region of the growth cone were even greater than those in growth cones treated with only control siRNA and vinblastine (mean ± SEM = 53.8 ± 5.6 AFU, $n = 17$; $p = 0.11$). Finally, when DHC siRNA was combined with the vinblastine and blebbistatin treatments, the microtubule mass in the distal region of the growth cone was similar to those in neurons treated with control siRNA, vinblastine and blebbistatin (mean ± SEM = 53.4 ± 5.41, $n = 15$) (Figure 9). Thus, the inhibition of myosin-II obliterated the reduction in microtubule mass observed with dynein depletion under these experimental conditions. Taken together, these results indicate that, even in the absence of microtubule assembly, the forces generated by cytoplasmic dynein are conducive to the invasion of microtubules into the peripheral zone, while the forces generated by myosin-II are antagonistic to this invasion. The fact that some of the microtubules do gain

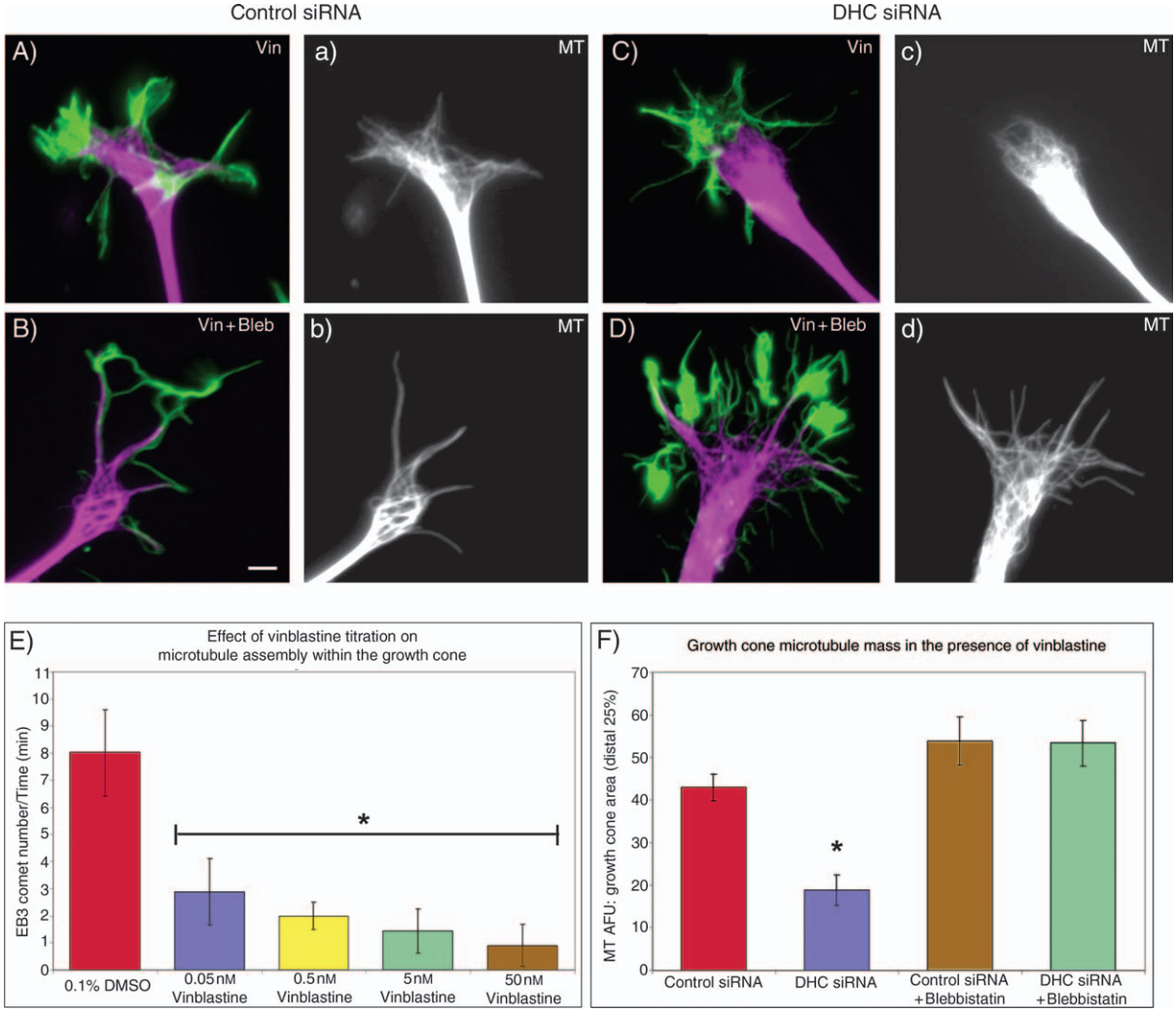

Figure 9: Depletion of DHC decreases distal growth cone microtubule mass when microtubule assembly is inhibited. A/a Images of control-siRNA-treated growth cones in the presence of vinblastine (Vin) alone to inhibit microtubule (MT) assembly. B/b) Control-siRNA-treated growth cones with a combined treatment of vinblastine and blebbistatin (Bleb) to inhibit microtubule assembly and myosin-II activity. In control growth cones treated with siRNA/vinblastine, the microtubules extend into the distal regions of the cone but do not appear to extend into filopodia. The combined vinblastine/blebbistatin treatment enhances distal microtubule levels, and microtubules can be clearly seen within growth cone filopodia. When DHC is depleted in the presence of vinblastine, the levels of distal microtubules are greatly reduced and appear primarily constrained to the central zone of the growth cone (C/c). Treatment with vinblastine/blebbistatin enhances levels of distal microtubules and facilitates their extension toward and into growth cone filopodia (D/d). E) Graph showing that microtubule dynamics are suppressed significantly and proportionally with increasing concentrations of vinblastine, as measured by the frequency of EGFP-EB3 comets appearing within the growth cone. Statistical comparison of vinblastine titrations with 0.1% DMSO revealed that each of the drug treatments resulted in a significant reduction in the number of EGFP-EB3 comets with respect to time (*, $p < 0.00003$, two-tailed *t*-test), with the 50 nM vinblastine treatment resulting in the most substantial suppression of microtubule dynamics ($p < 0.000004$; 0.1% DMSO versus 50 nM vinblastine; two-tailed *t*-test). F) Graph representing the relative levels of growth cone microtubule mass in the presence of vinblastine. Measurements of microtubule mass were calculated per unit area for the distal 25% of the growth cone and revealed that under conditions of DHC depletion alone, there was a 43.7% reduction in microtubule mass compared to neurons treated with control siRNA ($p < 0.00001$, two-tailed *t*-test; control, $n = 17$; DHC, $n = 16$). Addition of blebbistatin restored distal growth cone levels of microtubules to similar levels in cultures treated with both control ($n = 17$) and DHC siRNA ($n = 15$). These increases in distal microtubule mass were significantly different from the DHC siRNA group in the absence of blebbistatin (*, $p < 0.0001$, two-tailed *t*-test) but was not statistically different from the control siRNA group ($p > 1$, two-tailed *t*-test). A, B, C and D depict microtubules (violet) and phalloidin (green) staining. a, b, c and d represent the original anti-B-tubulin and Cy3-immunofluorescence images. Bar, 10 μm.

entry into the peripheral zone when both assembly and dynein-driven forces are suppressed suggests that there are probably kinesin-related motors that also contribute to force generation and microtubule organization within the growth cone (7,9).

Discussion

Cytoplasmic dynein was originally suggested to be the motor that transports axonal microtubules on the basis of the fact that it is conveyed down the axon at the same rate as actin (41). It was posited that dynein associates with the actin cytoskeleton indirectly via its cargo domain, thus leaving its motor domain available to intermittently interact with microtubules (42). Since this model was proposed, we have experimentally demonstrated that cytoplasmic dynein indeed transports microtubules anterogradely down the axon (7) and that at least some of these microtubules are transported by pushing against the actin cytoskeleton (8). The fact that only very short microtubules are transported raises the question as whether the dynein-driven forces between microtubules and actin filaments are selective for short microtubules or whether they impinge upon longer immobile microtubules as well. We have proposed the latter to be the case and have speculated on how such forces might be important for integrating microtubules and actin filaments during axonal retraction and growth cone turning (9,20).

The studies presented here demonstrate that dynein-depleted axons retract more dramatically than control axons when exposed to donors of nitric oxide and show major deficits in the capacity of their growth cones to turn on patterned substrates. Cytoplasmic dynein is a multifunctional motor protein, and it is certainly conceivable that these results might relate, at least in part, to factors other than force generation between microtubules and actin filaments. For example, growth factors relevant to axonal retraction and/or growth cone guidance may require dynein motors to transport them along the axon (43). In addition, the accumulation of organelles and neurofilaments that occurs during dynein depletion may have non-specific detrimental effects, particularly to growth cones. For these reasons, we conducted our experiments under conditions of partial dynein depletion that permit axons to grow at normal rates. Moreover, the deficit in the capacity of dynein-depleted growth cones to turn was apparent regardless of whether they had a spread morphology or a blunt morphology typically indicative of vesicle and neurofilament accumulations. Thus, while we cannot dismiss a possible contribution from other dynein-related factors, these considerations suggest that our observations reflect a more direct role for dynein-driven forces on the disposition of the microtubules.

With regard to axonal retraction, it has been known for decades that microtubules within the axonal shaft offset the tendency of the axon to retract by an actin-based mechanism (44,45). It was originally believed that it was merely the presence of the microtubules in the axon as architectural elements that prevented the axon from retracting because drugs that depolymerize microtubules cause axons to retract. However, the microtubules in axons retracting in response to physiological cues do not display any marked depolymerization but rather bend and retreat as the axon shortens (27). We previously demonstrated that an abrupt disruption of dynactin causes poorly adhered axons to spontaneously retract (23), and here, we have shown that depletion of dynein itself similarly renders axons more sensitive to retraction in response to nitric oxide. In both cases, the retraction was prevented if the neurons were treated with inhibitors of myosin-II, which is known to generate the forces that underlie the contractility of the cortical actin (10,11). On the basis of these results, it appears that whether the axon grows or retracts depends on the appropriate balance between dynein-driven and myosin-II-driven forces. Our view is that the cortical actin is under continuous contractile forces imposed by myosin-II, but this contractility is antagonized if long microtubules are functionally integrated with the actin meshwork via dynein-driven forces. A shift in either of the two motor-driven forces, diminution in dynein or elevation of myosin-II could be the means by which factors such as nitric oxide cause the axon to retract.

Such an antagonistic relationship between these two motors on these two cytoskeletal elements has precedent in other cell types (46) and may be a broad theme by which microtubules and the actin cytoskeleton are integrated and co-regulated. Our results suggest that this kind of relationship also exists in growth cones. The turning deficit displayed by dynein-depleted growth cones is correlated with a reduced capacity of growth cone microtubules to extend beyond the central zone into the peripheral region and filopodia. Normally, the microtubules invade the peripheral zone by aligning with the straight bundles of actin filaments that extend into filopodia (13). A number of studies suggest that microtubules invade filopodia by assembly of the microtubule rather than its transport (13–18,47). Thus, it might seem surprising that the microtubules would need forces generated by a molecular motor to enter the peripheral zone and invade filopodia. We initially considered the possibility that the inability of the microtubules to enter the peripheral zone may be a direct result of the suppression of their dynamics, as we observed a slowing of plus end excursions in dynein-depleted growth cones. The fact that the transport of short microtubules is reduced, for example, might lower the available pool of tubulin, and hence dampen the dynamics of the long microtubules. However, in a previous study, we found that plus end excursions were not slowed in the axonal shaft after dynein depletion and were actually slightly faster than in control axons (6). Moreover, if there were a shortage of tubulin subunits or if there were only an assembly-dependent mechanism of microtubule advance

into the peripheral growth cone, the blebbistatin treatment would not reverse the phenomenon so rapidly.

Therefore, it would appear that something unique about the growth cone slows the plus end excursions of the microtubules and prevents their entry into the peripheral zone when dynein is depleted. A major difference between the growth cone and the axonal shaft is that the growth cone is subjected to the retrograde flow of actin filaments fueled by myosin-II. The retrograde flow has been documented to sweep microtubules backward in growth cones under certain conditions (18,32,35,48), so it is reasonable that a force in addition to that generated by microtubule polymerization might be necessary for microtubules to overcome such backward sweeping forces and enter the peripheral zone of the growth cone. We posit that cytoplasmic dynein serves this role. Indeed, our results indicate that inhibition of myosin-II by blebbistatin permits microtubules in dynein-depleted growth cones to gain entry into the peripheral zone, to invade filopodia and to once again undergo rapid dynamics. These observations are consistent with a model whereby microtubule distribution in growth cones is regulated by a balance of forces generated by these two molecular motors.

The question arises as to exactly how this might work. Several studies have now established that microtubule assembly is required for the invasion of microtubules into filopodia during growth cone turning (33,39,40). One possibility is that the forces generated by cytoplasmic dynein are necessary within the filopodium itself to assist the microtubule in associating with the actin bundle as it assembles (9,20). In this model, as the actin bundle moves backward, the dynein-driven forces enable the microtubule to ratchet along the actin bundle in the opposite direction. Our studies on growth cones treated with vinblastine suggest another model in which the microtubules can penetrate from the central zone into the peripheral zone only if the dynein-driven forces are strong enough to overpower the myosin-II-driven forces. Then, once having entered the peripheral zone, the microtubules would have the potential to polymerize into filopodia. In the first model, the dynein-driven forces are important within the filopodia themselves, while in the second model, the dynein-driven forces are important in the lamellar region of the peripheral zone. In support of the second model, recent studies suggest that the myosin-II-based forces that pull backwards on the actin bundles within filopodia are generated mainly within the lamellar region of the peripheral zone (49). On this basis, it is appealing to speculate that the lamellar region of peripheral zone may be analogous to the cortical meshwork of actin along the axonal shaft in the sense that both would represent major sites of force opposition between cytoplasmic dynein and myosin-II. These two models are certainly not mutually exclusive, and it will be of great interest to ascertain exactly where in the growth cone the forces generated by these two motors are most critical for orchestrating the microtubule behaviors the underlie axonal navigation.

Materials and Methods

Cell culture and transfection

Cultures of dissociated neurons from rat superior cervical ganglia were prepared as previously described (7). After dissociation by trituration, the cells were transfected by electroporation and then plated in N2 medium at a density of 7500 cells/cm^2 on glass cover slips mounted in the bottom of drilled 35-mm-diameter plastic Petri dishes whose glass bottoms had been treated for 3 h with 0.1 mg/mL poly-D-lysine. At least 3 h prior to imaging, the medium was replaced with pre-warmed L-15 plating medium, which has the advantage of maintaining pH in air. The L-15 contained 25 μg/mL laminin to stimulate the rapid outgrowth of axons. Two days after plating, by which time the DHC was reduced by over 70%, the neurons were released from the substratum and then replated either on a laminin-striped cover slip (for the turning assay, see below) or once again on polylysine-treated cover slips to which laminin was added (for the EB3-imaging, see below). Plasmid and/or siRNA for DHC or control siRNA was also introduced at the time of the initial plating by electroporation as previously described (6–8). The plasmids included an EGFP-EB3 plasmid provided by Dr Niels Galjart (30) and an mRFP-EB3 plasmid provided by Dr James Zheng. Corresponding controls were cultures expressing only the EGFP or mRFP tags with control siRNA.

Nitric oxide-induced axonal retraction

Sympathetic neurons were nucleofected with control or DHC siRNA and plated as described above. Two days after nucleofection, neurons were replated onto glass bottom culture dishes with grid treated with poly-D-lysine and laminin. By 7 h after replating, neurons had generated extensive axons. NOC-7 (Calbiochem, San Diego, CA, USA), was prepared and applied as previously described (27), except that it was used at a working concentration of 3 mM to elicit significant axonal retraction under the current culture conditions. In some experiments, 50 μM blebbistatin, a potent inhibitor of myosin-II, was added to the cultures 30 min prior to the introduction of the NOC-7. Phase-contrast images of axons were recorded before and 30 min after addition of NOC-7. Axonal lengths (from growth cone to cell body or to the first bifurcation point) were measured using the 'arbitrary curve measuring tool' in AXIOVISION. Raw data were processed, and graphs were produced using Excel (Microsoft Corp, Redmond, WA, USA). The means of retracted distances were compared using the two-tailed, unpaired Student's *t*-test. A p value of <0.05 was used as the standard for statistical significance in this study.

Stripe assay for growth cone turning

To assay growth cone turning, neurons transfected with control or DHC siRNA were cultured for 2 days and then replated onto a patterned laminin substrate consisting of alternating stripes of laminin-containing and laminin-free zones. The patterned substrate was prepared as previously described (29). Neurons plated onto the patterned substrate were allowed to extend axons for ≈15 h, at which time they were fixed and stained for laminin, microtubules and actin filaments. Color overlays were prepared from images of growth cones stained to reveal microtubules and actin filaments, and growth cones were scored as having no filopodia with microtubules or one or more filopodia with microtubules. In collecting these data, we evaluated separately growth cones at borders between laminin-containing and laminin-free zones and growth cones on laminin away from the borders and detected no difference in terms of microtubule invasion into filopodia and the effects of dynein depletion on this parameter. We therefore pooled the data from these two groups of growth cones and compared them statistically using the chi-square test. In many situations, turning was complete at the time of fixation and appeared as a relatively abrupt change in axonal orientation at or near the border. In these situations, turning was obvious. In other situations, growth cones were situated at borders without

a clear change in axonal orientation. In these cases, growth cones were categorized as turning or not turning based on the orientation of the growth cone microtubule array relative to that in the axon just proximal to the growth cone. Most of the microtubule polymer in the growth cone corresponds to the distal portions of much longer microtubules that extend from the axon into the growth cone. When the portion of these microtubules in the growth cone had an orientation that clearly differed from that in the axon, the growth cones were defined as turning, whereas they were defined as not turning when such a difference was not apparent. These microtubule-based criteria are useful because they can distinguish *bona fide* turning from the phenomenon of 'sidestepping' (14). While there is some subjectivity in distinguishing between these two behaviors on the basis of still images, any error would apply equally to control and dynein-suppressed neurons, and hence would not diminish the basic finding that dynein depletion retards growth cone turning.

Fluorescence procedures on fixed cells

For growth cone turning experiments, post-fixation fluorescence microscopy was used to obtain information on the distribution of microtubules and actin filaments in growth cones at borders between laminin-containing and laminin-free zones. For triple-label fluorescence microscopy of microtubules, actin filaments and laminin, cultures were simultaneously fixed and extracted by incubation for 10 min at room temperature with 1× PEM [80 mM piperazine-N,N′-bis[2-ethanesulfonic acid] (PIPES), 5 mM EGTA, 1 mM $MgCl_2$, pH 6.8.] containing 0.5% (octylphenoxy) polyethoxyethanol octylphenyl-polyethylene glycol CA-630 and 0.3% glutaraldehyde. Cells were then rinsed extensively in PBS, pH 7.4, further permeabilized by incubation with 0.5% Triton-X-100 in PBS for 15 min and then treated twice with 10 mg/mL sodium borohydride in PBS, 7 min each time, to quench glutaraldehyde-related autofluoresence. Samples were blocked by incubation for 30 min with 10 mg/mL BSA + 10% normal donkey serum, in PBS, and then incubated with primary antibodies, diluted in PBS, for 60 min at room temperature, rinsed extensively with PBS and reblocked for at least 10 min before incubation with secondary antibodies, diluted in PBS, for 45 min at room temperature. After extensive rinsing in PBS, samples were mounted in a medium that reduces photobleaching (0.212% *N*-propylgallate in 90% glycerol and 10% PBS).

Actin filaments were revealed using Alexa Fluor 488 phalloidin (Molecular Probes, Eugene, OR, USA) included with secondary antibodies and used at 1:40 dilution. Microtubules were revealed using DM1 alpha antibody, provided by Dr V. Gelfand, University of Illinois, diluted 1:1000, and Cy5-labeled donkey anti-mouse secondaries (diluted 1:50). Laminin was revealed using rabbit anti-laminin (Sigma, Atlanta, GA, USA) diluted 1:200, and Rhodamine Red-X-labeled donkey anti-rabbit secondaries (diluted 1:2000). Samples were observed on an Axiovert 200M inverted microscope (Carl Zeiss, Thornwood, NY, USA), and images were acquired using a Princeton Instruments cooled charge-coupled device (CCD) camera (Roper Scientific, Duluth, GA, USA) equipped with a back-thinned chip using IPLAB software (BD Biosciences, Rockville, MD, USA) to control the camera and other peripheral devices. Images were acquired using the full usable area of the CCD chip, which measured 1000 × 800 pixels and stored in full 12-bit format for processing and analysis. To reveal the general morphology of sympathetic neurons and to quantify total axonal length, fluorescent images were taken with a 25×/0.8 Plan-Neofluar oil objective; axon length was measured with the length-measuring tool in IPLAB. High-resolution images of growth cones were obtained with the 100×/1.3 Plan-Neofluar oil objective. For blebbistatin and vinblastine immunostaining experiments, cultured sympathetic neurons were fixed and microtubule and phalloidin staining was performed as previously described (8).

We compared the proportion of total growth cone area occupied by microtubules in control and dynein-deficient neurons. As these analyses were fairly tedious, they were performed on a subset of images from the experiment shown in Table 1. To avoid bias in the selection, the images were selected from the image list prior to viewing, and all spread growth cones in each image were analysed. We focused specifically on spread growth cones for these analyses for two reasons. First, even though spread growth cones of dynein-depleted neurons are deficient at turning compared to controls, the range of morphologies exhibited by spread growth cones is similar for both control and dynein-depleted neurons. Second, the analysis requires images in sharp focus to obtain accurate area measurements, and such images are readily obtained from spread growth cones because they are relatively flat. In contrast, the blunt growth cones are too thick to capture in good focus in single images. Growth cone area was calculated from images of actin filament staining, and microtubule area was calculated based on the image of microtubule staining. Actin filament and microtubule images were flat field corrected. A threshold was then applied to the images to produce a binary image that faithfully represented the stained image, and area measurements were obtained from the binary images. The proportion of total growth cone area occupied by microtubules was obtained by dividing microtubule area with growth cone area, and the resulting values were compared statistically using Student's *t*-test.

EGFP-EB3 or mRFP-EB3 live cell imaging

All the live cell imaging was performed using an AxioVert 200M inverted microscope (Carl Zeiss) coupled either to an Orca-ER or to an Orca II-ER Digital CCD Camera (Hamamatsu Corp, Hamamatsu City, Japan). The CCD camera and most aspects of the microscope were controlled by AXIOVISION version 3.0 or 4.5 software (Carl Zeiss) running on either a Pentium II-based computer (Tekgraf) with the Windows 2000 operating system (Microsoft Corp) or an Intel Xeon processor-based computer (Fujitsu America, Sunnyvale, CA, USA) with the Windows XP Professional operating system (Microsoft Corp). Images were obtained using a 100× Plan-Neofluar/1.3 NA or a 100×/1.3NA Plan Apo oil immersion objective (Carl Zeiss). Temperature of the cultures was maintained at 37°C with the use of a Tempcontrol 37-2 digital heated stage and controller and a Tempcontrol-mini heated objective lens collar and controller (Carl Zeiss). Excitation of fluorescent molecules and collection of correct emission wavelengths were accomplished with an AttoArc 2 or a FluoArc Variable Intensity HBO 100 Arc Lamp Control (Atto Instruments, Rockville, MD, USA), a 100-watt mercury vapor lamp and the appropriate excitation and emission filters and dichroic mirrors (Chroma, Rockingham, VT, USA). To acquire images for live cell time-lapse movies, neutral density filters were placed in the illuminating light path or the output of the variable intensity mercury lamp was adjusted to reduce photobleaching and photodamage of the sample. In some experiments, cultures were exposed to 50 μM blebbistatin to inhibit myosin-II functions. Imaging began 10 min after the introduction of the drug and never exceeded a 1 h in the presence of the drug.

Images were acquired at a rate of 1 per second excluding camera exposure times for time-lapse movies. Depending on the intensity of the EB3 fluorescence signal, exposure times ranged from 200 to 700 mseconds such that real-time imaging of individual growth cones ranged from 5 to 7 min. To maximize the fluorescent signal while minimizing exposure times, the CCD camera was set to 2 × 2 binning, with the gain set to 1.5, the gain offset at 0 and the gain factor equal to 2. Frames extracted for still images were exported from AXIOVISION as TIFF image files and processed in PHOTOSHOP 7 (Adobe Corp, San Jose, CA, USA). All EGFP-EB3 quantification was performed using the AXIOVISION 'measure' module. Measurements of comet frequency within growth cone filopodia were analysed over the first 5 min of the imaging sequence as a method for normalization to time. Raw data were processed and graphs/charts were produced using Excel (Microsoft Corp). For EB3/filopodial invasion analysis, individual filopodia were scored only if their lengths were 5 μm or greater at the start of imaging. Filopodial length measurements were taken from the distal tip back to the position of the growth cone at which the filopodium originated, and a line perpendicular to the distal filopodium tip was drawn at this position to demarcate the point of origin and to facilitate excursion depth analysis. EB3 excursion depth data included measurements of comets that crossed the filopodia origin line and EB3 comets arising from within individual filopodia, all of which were measured back to the filopodia origin line. Depth measurements were recorded from the deepest excursion point at which the EB3 comet remained visible. EB3 excursion velocities were calculated as the distance moved by individual EB3 comets

over three frame intervals, divided by the time that individual comets remained visible. Kymographs were generated for individual EB3 comets in METAMORPH version 6.2r1 (Molecular Devices Inc, Downingtown, PA, USA) using the 'kymograph' function and were recorded for 35 seconds using a line width parameter equal to 3, with the line length set to 12 pixels (5 μm).

For vinblastine titration experiments, neurons were cultured as described above and transfected with either control or DHC siRNA and EGFP-EB3 (10 μg), plated onto 35-mm plastic dishes coated with poly-D-lysine in L-15 plating medium supplemented with laminin (final concentration 5 μg/mL) and allowed to grow for 2 days before being replated onto poly-D-lysine-coated special dishes. The following morning, the replated neurons were treated with 5 μg/mL of laminin. Drug treatments were diluted to their respective concentrations in L-15 plating medium and then added to the culture dish 30 min prior to the start of EGFP-EB3 imaging. Imaging of EB3 comets was conducted as described above except that the exposure time for all movies was kept at 800 mseconds and the total length of individual movies was 3 min. Data analysis of control siRNA and DHC siRNA groups showed no difference with respect to mean comet number within growth cones for individual vinblastine concentrations ($p > 0.05$, two-tailed *t*-test). Statistical analyses were performed in Microsoft Excel and represent the combination of both control and DHC siRNA data sets [$n = 12$, 0.1% dimethyl sulphoxide (DMSO); $n = 9$, 0.05–5 nM vinblastine; $n = 10$, 50 nM vinblastine].

Bead preparation and live cell imaging of retrograde flow in growth cones

The 535-nm carboxylated polystyrene beads (Polysciences Inc., Warrington, PA, USA) were conjugated to polyethylenamine using the carbodiimide conjugation protocol provided by the manufacturer (Polysciences Technical Data Sheet 238C) and a 5% polyethylenamine aqueous solution. We chose to conjugate the beads to polyethylenamine because it has been shown to facilitate bead interactions with the growth cone and more importantly because there are no visible secondary effects to growth cone morphology or extension rates, as have been reported both for other polyamines and for growth factors (17,50). Sympathetic neurons were cultured as described (8) with minor modifications. Briefly, neurons were cultured following transfection with either control or DHC siRNA, replated 2 days later onto poly-D-lysine-coated dishes and allowed to grow overnight. The next morning, neurons were treated with 1:200 dilution of laminin (final concentration, 5 μg/mL) in L-15 plating medium. When a sufficient number of growth cones were visible (typically 3–5 h after laminin addition), the medium was removed entirely and replaced with 200 μL of L-15 plating medium containing 1:1000 dilution of conjugated beads. The dish was then incubated at 37°C for 10 min to allow the beads to settle to the bottom of the dish. Live cell imaging was performed using an AxioVert 200M inverted microscope (Carl Zeiss) coupled to an Orca-ER Digital CCD Camera (Hamamatsu, Japan). The CCD camera and most aspects of the microscope were controlled by AXIOVISION version 3.0 (Carl Zeiss) running on a Pentium II-based computer (Tekgraf) with the Windows 2000 operating system (Microsoft Corp). Conjugated beads that were observed to bind to the growth cone and to move primarily from the distal growth cone retrogradely toward the central region of the cone were chosen for analysis. Beads located in the central region of the growth cone or beads that did not appear to move during the duration of image acquisition were excluded from image analysis. Differential Interference Contrast (DIC) movie frames were acquired at 5-second intervals for a total duration of 5 min (61 cycles), with a 30-mseconds exposure time, the gain equal to 0 and no binning. Image analysis was performed using the 'track objects' function of METAMORPH software version 6.2r1 (Molecular Devices Inc), and data points were exported to Microsoft Excel (Microsoft Corp).

Growth cone microtubule mass experiments

Sympathetic neurons were cultured and replated as described for retrograde flow experiments with the following exceptions. The morning after replating, neurons were treated with 50 nM vinblastine for 30 min, followed by treatment with 50 nM vinblastine and 1:200 dilution of laminin (final concentration, 5 μg/mL) for 2 h. For the blebbistatin experimental groups, 50 μM blebbistatin was added to the culture dishes 30 min prior to fixation (1.5 h after addition of the vinblastine/laminin). Concentrations of laminin and vinblastine were kept constant regardless of the treatment conditions. All drug/laminin treatments were diluted in L-15 plating medium that was added by removing 1 mL of plating medium (half the total volume) from the culture dish and replacing it with 1 mL of the respective drug/laminin (2× concentration). Following the completion of all drug treatments, the dishes were fixed and stained for actin and microtubules as described above in fluorescence procedures for fixed cells. Images were obtained using a 100× Plan-Neofluar/1.3 NA or a 100×/1.3NA Plan Apo oil immersion objective (Carl Zeiss) using the microscope systems described above. Acquisition settings were maintained at a constant rate enable accurate evaluation of fluorescence intensity. For microtubule staining, images were acquired in AXIOVISION version 4.5 using a 20-msecond exposure time, with the gain set to 255 and the gain offset at 0. For phalloidin staining, images were acquired using a 200-msecond exposure time, with 255 gain and gain offset equal to 0. Image analysis and processing were performed using METAMORPH software version 6.2r1 (Molecular Devices Inc). Briefly, individual microtubule and actin staining images were overlayed using the 'image overlay' function of METAMORPH, and the total growth cone area was measured using the 'outline tool' to trace the outline of growth cone phalloidin staining. A 'journal' was created in METAMORPH through which we could alter the size of our growth cone outline to any percent of its original size. Using the 'run journal' function to initiate this journal, we then reduced the original outline to 75% of its size, and microtubule fluorescence intensity and area measurements were calculated for both growth cone areas using the 'region measurements' tool. Data were exported to Microsoft Excel (Microsoft Corp), and the fluorescence values for the 75% were subtracted from the total growth cone fluorescence values (100%) to obtain fluorescence intensity for the distal 25% of the growth cone. These fluorescence measurements were then normalized to growth cone area measurements to obtain AFU/area for the distal 25% of the growth cone.

Final processing for all figure images was performed using ADOBE PHOTOSHOP version 7 (Adobe Corp.).

Acknowledgments

This work was supported by grants from National Institutes of Health (NIH) to P. W. B. and M. M. B., Tobacco Settlement Funds to P. W. B. and M. M. B. from the State of Pennsylvania and a grant from the Alzheimer's Association to P. W. B. K. A. M. is supported by a predoctoral National Research Service Award (NRSA) from the NIH. I. T. is supported by a Postdoctoral Training Grant from the NIH. We thank Niels Galjart for providing the EGFP-EB3 construct and James Zheng for providing the mRFP-EB3 construct. We are appreciative to Andrew Schaefer, Thomas Hasaka and Gianluca Gallo for their helpful advice and discussions.

Supplementary Materials

Movie S1: Control-siRNA-treated growth cone of a rat sympathetic neuron transfected with EGFP-EB3. The EB3 comets emanating from the central zone of the growth cone are observed to consistently enter growth cone filopodia and progress toward their distal tips. The frames were acquired every 1 second for 3 min.

Movie S2: Dynein-depleted growth cone of a rat sympathetic neuron transfected with EGFP-EB3. Unlike the control growth cone, not many comets progress outward from the central zone. A few EB3 comets can be seen in the peripheral zone but are unable to gain entrance into filopodia.

The retrograde flow of actin, which may be representative of myosin-II-driven forces manifested in the absence of dynein-based oppositional forces, is shown particularly well in this movie. The frames were acquired every 1 second for 3 min.

Movie S3: Dynein-depleted growth cone of a rat sympathetic neuron transfected with mRFP-EB3 and treated with 0.1% DMSO for 10 min. The comets are seen only in the central zone and are unable to invade filopodia, reminiscent of EGFP-EB3 comets under conditions of dynein depletion (Movie S2). The frames were acquired every 1 second for 2 min.

Movie S4: Dynein-depleted growth cone of a rat sympathetic neuron treated with 50 μM blebbistatin for 10 min to inhibit the activity of myosin-II. Comets arise in the central region of the growth cone and consistently invade filopodia, progressing toward the distal tips of filopodia in a manner similar to neurons treated with control siRNA alone (Movie S1), are shown. These data support the hypothesis that the inhibition of myosin-II serves to relieve dynein-based inhibition of microtubule invasion of filopodia. The frames were acquired every 1 second for 2 min

Supplemental materials are available as part of the online article at http://www.blackwell-synergy.com

References

1. Baas PW, Ahmad FJ. The plus ends of stable microtubules are the exclusive nucleating structures for microtubules in the axon. J Cell Biol 1992;116:1231–1241.
2. Brown A, Li Y, Slaughter T, Black MM. Composite microtubules of the axon: quantitative analysis of tyrosinated and acetylated tubulin along individual axonal microtubules. J Cell Sci 1993;104:339–352.
3. Yu W, Baas PW. Changes in microtubule number and length during axon differentiation. J Neurosci 1994;14:2818–2829.
4. Wang L, Brown A. Rapid movement of microtubules in axons. Curr Biol 2002;12:1496–1501.
5. Ma Y, Shakiryanova D, Vardya I, Popov SV. Quantitative analysis of microtubule transport in growing nerve processes. Curr Biol 2004;14:725–730.
6. Ahmad FJ, He Y, Myers KA, Hasaka TP, Francis F, Black MM, Baas PW. Effects of dynactin disruption and dynein depletion on axonal microtubules. Traffic 2006;7:524–537.
7. He Y, Frances F, Myers KA, Yu W, Black MM, Baas PW. Role of cytoplasmic dynein in the axonal transport of microtubules and neurofilaments. J Cell Biol 2005;168:697–703.
8. Hasaka TP, Myers KA, Baas PW. Role of actin filaments in the axonal transport of microtubules. J Neurosci 2004;24:11291–11301.
9. Baas PW, Nadar CV, Myers KA. Axonal microtubule transport: the long and short of it. Traffic 2006;7:490–498. [Review].
10. Gallo G. Myosin II activity is required for severing-induced axon retraction in vitro. Exp Neurol 2004;189:112–121.
11. Gallo G, Yee HF Jr, Letourneau PC. Actin turnover is required to prevent axon retraction by endogenous actomyosin activity. J Cell Biol 2002;158:1219–1228.
12. Baas PW, Ahmad FJ. Force generation by cytoskeletal motor proteins as a regulator of axonal elongation and retraction. Trends Cell Biol 2001;11:244–249. [Review].
13. Zhou FQ, Cohan CS. How actin filaments and microtubules steer growth cones to their targets. J Neurobiol 2004;58:84–91. [Review].
14. Tanaka E, Kirschner MW. The role of microtubules in growth cone turning at substrate boundaries. J Cell Biol 1995;128:127–137.
15. Challacombe JF, Snow DM, Letourneau PC. Actin filament bundles are required for microtubule reorientation during growth cone turning to avoid an inhibitory guidance cue. J Cell Sci 1996;109:2031–2040.
16. Buck KB, Zheng JQ. Growth cone turning induced by direct local modification of microtubules. J Neurosci 2002;22:9358–9367.
17. Suter DM, Schaefer AW, Forscher P. Microtubule dynamics are necessary for SRC family kinase-dependent growth cone steering. Curr Biol 2004;14:1194–1199.
18. Schaefer AW, Kabir N, Forscher P. Filopodia and actin arcs guide the assembly and transport of two populations of microtubules with unique dynamic parameters in neuronal growth cones. J Cell Biol 2002;158:139–152.
19. Zhou FQ, Waterman-Storer CM, Cohan CS. Focal loss of actin bundles causes microtubule redistribution and growth cone turning. J Cell Biol 2002;157:839–849.
20. Myers KA, He Y, Hasaka TP, Baas PW. Microtubule transport in the axon: re-thinking a potential role for the actin cytoskeleton. Neuroscientist 2006;12:107–118. [Review].
21. Dehmelt L, Halpain S. Actin and microtubules in neurite initiation: are MAPs the missing link? J Neurobiol 2004;58:18–33. [Review].
22. Maskery S, Shinbrot T. Deterministic and stochastic elements of axonal guidance. Annu Rev Biomed Eng 2005;7:187–221. [Review].
23. Ahmad FJ, Hughey J, Wittmann T, Hyman A, Greaser M, Baas PW. Motor proteins regulate force interactions between microtubules and microfilaments in the axon. Nat Cell Biol 2000;2:276–280.
24. Deacon SW, Serpinskaya AS, Vaughan PS, Lopez Fanarraga M, Vernos I, Vaughan KT, Gelfand VI. Dynactin is required for bidirectional organelle transport. J Cell Biol 2003;160:297–301.
25. Schroer TA. Dynactin. Annu Rev Cell Dev Biol 2004;20:759–779. [Review].
26. Vallee RB, Williams JC, Varma D, Barnhart LE. Dynein: an ancient motor protein involved in multiple modes of transport. J Neurobiol 2004;58:189–200. [Review].
27. He Y, Yu W, Baas PW. Microtubule reconfiguration during axonal retraction induced by nitric oxide. J Neurosci 2002;22:5982–5991.
28. Turney SG, Bridgman PC. Laminin stimulates and guides axonal outgrowth via growth cone myosin II activity. Nat Neurosci 2005;8:717–719.
29. Bouquet C, Soares S, von Boxber Y, Ravaille-Veron M, Propst F, Nothias F. Microtubule-associated protein 1B controls directionality of growth cone migration and axonal branch regeneration of adult dorsal root ganglia neurons. J Neurosci 2004;24:7204–7213.
30. Stepanova T, Slemmer J, Hoogenraad CC, Lansbergen G, Dortland B, De Zeeuw CI, Grosveld F, van Cappellen G, Akhmanova A, Galjart N. Visualization of microtubule growth in cultured neurons via the use of EB3-EGFP (end-binding protein 3-green fluorescent p rotein). J Neurosci 2003;23:2655–2664.
31. Wu X, Xiang X, Hammer JA III. Motor proteins at the microtubule plus-end. Trends Cell Biol 2006;16:135–143. [Review].
32. Lin CH, Forscher P. Growth cone advance is inversely proportional to retrograde F-actin flow. Neuron 1995;16:769–782.
33. Suter DM, Forscher P. Substrate-cytoskeletal coupling as a mechanism for the regulation of growth cone motility and guidance. J Neurobiol 2000;44:97–113.
34. Brown J, Bridgman PC. Role of myosin II in axon outgrowth. J Histochem Cytochem 2003;51:421–428.
35. Lin CH, Espreafico EM, Mooseker MS, Forscher P. Myosin drives retrograde F-actin flow in neuronal growth cones. Neuron 1996;16:769–782.
36. Bridgman PC. Growth cones contain myosin II bipolar filament arrays. Cell Motil Cytoskeleton 2002;52:91–96.
37. Brown ME, Bridgman PC. Myosin function in nervous and sensory systems. J Neurobiol 2004;58:118–130.
38. Kolega J. Phototoxicity and photoinactivation of blebbistatin in UV and visible light. Biochem Biophys Res Commun 2004;320:1020–1025.

39. Tanaka E, Ho T, Kirschner MW. The role of microtubule dynamics in growth cone motility and axonal growth. J Cell Biol 1995;128:139–155.
40. Challacombe JF, Snow DM, Letourneau PC. Dynamic microtubule ends are required for growth cone turning to avoid an inhibitory guidance cue. J Neurosci 1997;17:3085–3095.
41. Dillman JF III, Dabney LP, Karki S, Paschal BM, Holzbaur EL, Pfister KK. Functional analysis of dynactin and cytoplasmic dynein in slow axonal transport. J Neurosci 1996;16:6742–6752.
42. Pfister KK. Cytoplasmic dynein and microtubule transport in the axon: the action connection. Mol Neurobiol 1999;20:81–91. [Review].
43. Heerssen HM, Pazyra MF, Segal RA. Dynein motors transport activated Trks to promote survival of target-dependent neurons. Nat Neurosci 2004;7:596–604.
44. Yamada KM, Spooner BS, Wessells NK. Ultrastructure and function of growth cones and axons of cultured nerve cells. J Cell Biol 1971; 49:614–635.
45. Solomon F, Magendantz M. Cytochalasin separates microtubule disassembly from loss of asymmetric morphology. J Cell Biol 1981;89:157–161.
46. Yvon AM, Gross DJ, Wadsworth P. Antagonistic forces generated by myosin II and cytoplasmic dynein regulate microtubule turnover, movement, and organization in interphase cells. Proc Natl Acad Sci U S A 2001;98:8656–8661.
47. Dent EW, Kalil K. Axon branching requires interactions between dynamic microtubules and actin filaments. J Neurosci 2001;21:9757–9769.
48. Brown ME, Bridgman PC. Retrograde flow rate is increased in growth cones from myosin IIB knockout mice. J Cell Sci 2003;116:1087–1094.
49. Medeiros NA, Burnette DT, Forscher P. Myosin II functions in actin-bundle turnover in neuronal growth cones. Nat Cell Biol 2006;8: 215–226.
50. Grabham PW, Foley M, Umeojiako A, Goldberg DJ. Nerve growth factor stimulates coupling of beta1 integrin to distinct transport mechanisms in the filopodia of growth cones. J Cell Sci 2000;113:3003–3012.